Corrected 22 December 2021. See full text.

RADIATIVE COOLING

Scalable thermochromic smart windows with passive radiative cooling regulation

Shancheng Wang[1,2]†, Tengyao Jiang[3,4]†, Yun Meng[1,2], Ronggui Yang[5]*, Gang Tan[3]*, Yi Long[1,2,6]*

Radiative cooling materials spontaneously radiate long-wave infrared (LWIR) to the cold outer space, providing cooling power that is preferred in hot seasons. Radiative cooling has been widely explored for walls and roofs but rarely for windows, which are one of the least energy-efficient parts of buildings. We fabricated scalable smart windows using a solution process giving different emissivity (ε) at high ($\varepsilon_{LWIR\text{-}H}$ of 0.61) and low ($\varepsilon_{LWIR\text{-}L}$ of 0.21) temperatures to regulate radiative cooling automatically while maintaining luminous transparency and near-infrared (NIR) modulation. These passive and independent visible–NIR–LWIR regulated smart windows are capable of dynamic radiative cooling for self-adapting applications across different climate zones.

Buildings consume ~40% of global energy, and windows, one of the least energy-efficient parts, account for as much as 60% of their energy loss (*1*–*3*). In the United States, the window-associated heating and cooling energy consumption in buildings has been estimated at 4% of nation's total primary energy usage (*4*). Thermochromic windows are considered a cost-effective, stimulirational, energy-efficient smart window because of their simple structure, passive light modulation, and zero-energy input characteristics (*5*–*7*). The performance indexes of smart windows are luminous transmission (T_{lum}) and solar transmission modulation (ΔT_{sol}), where ΔT_{sol} is defined as the difference in T_{sol} (0.38 to 2.5 μm) between low and high temperatures (Fig. 1A) (*8*). However, the modulation of emissivity (ε) of long-wave infrared (ε_{LWIR}, 2.5 to 25 μm) in windows has rarely been studied.

Radiative cooling (RC) through LWIR spontaneously cools a surface by radiating thermal heat to the cold outer space. In recent years, there have been several applications using this strategy, including a subambient radiative cooler (*9*–*14*), energy-saving film (*15*), RC-based air-conditioning system (*16*–*18*), fabrics (*19*), roof (*20*), and energy-saving paint (*21*) (table S1). However, the fixed high ε_{LWIR} can only provide cooling when the weather is warm. Modulated RC catering to different seasonal weather conditions is needed for regions with hot and cold seasonal temperature fluctuations.

We propose a set of characteristics for an ideal smart window (Fig. 1A) that should have transparency in the visible range (380 to 780 nm) for both low and high temperatures. The T_{sol} has contributions from both the visible and near IR (NIR, 0.78 to 2.5 μm) ranges, which is responsible for heating a room. Changing the NIR state from opaque in the summer to transparent in winter is therefore desirable. Moreover, an ideal smart window should have a high ε_{LWIR} at high temperature ($\varepsilon_{LWIR\text{-}H}$) to promote RC during warm weather and a low ε_{LWIR} at low temperature ($\varepsilon_{LWIR\text{-}L}$) to suppress RC when it is cold outside.

Tuning ε_{LWIR} has been discussed theoretically (*22*–*24*) and demonstrated experimentally (*25*–*27*). However, these experiments tuned the ε_{LWIR} in an opposite way from what is helpful for windows (i.e., low $\varepsilon_{LWIR\text{-}H}$ and high $\varepsilon_{LWIR\text{-}L}$). We developed a transparent, passive RC regulating thermochromic (RCRT) smart window using near room temperature phase change vanadium dioxide (VO_2) and doped VO_2. We aimed to regulate both NIR transmission and RC spontaneously. Such an RCRT window fabricated by a solution process achieves luminous transparency with ΔT_{sol} (9.3%) and $\Delta\varepsilon_{LWIR}$ (defined as the difference between $\varepsilon_{LWIR\text{-}L}$ and $\varepsilon_{LWIR\text{-}H}$) of 0.4. Our energy consumption simulations suggest that the RCRT window gives a higher energy saving than commercial low-E glass across different climate zones.

For our RCRT window, the NIR is blocked in summer to prevent solar heating while the visible transparency remains unchanged (Fig. 1B). This is different from hydrogel-based smart windows, which turn opaque in the summer (*28*, *29*). Because RCRT windows have a high front side LWIR emissivity ($\varepsilon_{LWIR\text{-}H,Front}$), the RC helps to lower the cooling load further. In winter, both visible and NIR are transmitted while $\varepsilon_{LWIR\text{-}L,Front}$ is switched to lower values, reducing RC heat loss. Here, we kept $\varepsilon_{LWIR\text{-}Back}$ low in both conditions to minimize the heat exchange between the indoors and outdoors.

We designed and fabricated our RCRT window using spin coating, resulting in VO_2/spacer/low-E stacking (Fig. 1C) to form a Fabry-Perot resonator (*30*). Such a resonator has low resonance to the LWIR at low temperature but shows a strong Fabry-Perot resonation effect to give much-enhanced LWIR absorption due to the insulator-to-metallic transformation of VO_2 (*31*). The stacking consists of a VO_2 nanocomposite overcoat (Fig. 1D), a poly(methyl methacrylate) (PMMA) lossless spacer layer due to high solar and LWIR transparency (fig. S1), and two layers of indium tin oxide (ITO) low-E coating due to its high visible transmittance (~80%; fig. S2) and low ε_{LWIR} (~0.1; fig. S3). The VO_2 nanoparticles (figs. S4 to S6) are dispersed in PMMA solution and spin coated on PMMA spacer, serving the core functionality of T_{sol} and RC modulation. We compared photos of two transparent smart windows with and without RC regulation with the size up to 5 × 5 cm at both low and high temperatures (Fig. 1E). This solution-based fabrication process provides the potential for scaling up to building-sized windows.

We determined the optical spectra of our RCRT window (Fig. 2A) with T_{lum} of 27.8 and 26.1% at 20° and 90°C, respectively, and a ΔT_{sol} of 9.3%. The low transmittance of wavelength longer than 1500 nm was caused by the strong NIR blocking of the ITO coating (fig. S7). The transition temperature (τ_c) of the VO_2 layer was ~60°C, which can be tuned through doping (fig. S8). The RCRT window showed a promising ε_{LWIR} switching performance. At 20°C, the multilayer structure had a ε_{LWIR} of 0.21 and increased to 0.61 above τ_c, with a $\Delta\varepsilon_{LWIR}$ of 0.40. As a comparison, the spectra of the VO_2 sample without RC regulation (Fig. 2B) gives a typical T_{lum} of 32.2% and ΔT_{sol} of 17% but a negligible $\Delta\varepsilon_{LWIR}$ ($\varepsilon_{LWIR\text{-}L}$: 0.82, $\varepsilon_{LWIR\text{-}H}$: 0.85). The stacking design (Fig. 1D) leads to the favorable $\Delta\varepsilon_{LWIR}$ (Fig. 2A).

We collected images with an IR camera of both samples (Fig. 2C) with the background ε_{LWIR} of 0.5. We observed that from 30° to 60°C, the RCRT window was darker than the background, indicating a lower ε_{LWIR} compared with background (0.21 versus 0.5) because high ε_{LWIR} gives high thermal radiation intensity. With temperature above 70°C, the RCRT window turned brighter than the background because of a higher ε_{LWIR} compared with background (0.61 versus 0.5). By contrast, the sample with no RC regulation showed a constant brighter color than the background, which further demonstrates that it fails to modulate its ε_{LWIR} without structure manipulation.

[1]School of Materials Science and Engineering, Nanyang Technological University, Singapore, 639798, Singapore. [2]Singapore-HUJ Alliance for Research and Enterprise (SHARE), Campus for Research Excellence and Technological Enterprise (CREATE), Singapore, 138602, Singapore. [3]Department of Civil and Architectural Engineering and Construction Management, University of Wyoming, Laramie, WY 82071, USA. [4]School of Environmental Science and Engineering, Nanjing Tech University, Nanjing, Jiangsu 211816, China. [5]State Key Laboratory of Coal Combustion, School of Energy and Power Engineering, Huazhong University of Science and Technology, Wuhan, Hubei 430074, China. [6]Sino-Singapore International Joint Research Institute (SSIJRI), Guangzhou 510000, China. ***Corresponding author. Email: longyi@ntu.edu.sg (Y.L.); gtan@uwyo.edu (G.T.); ronggui@hust.edu.cn (R.Y.)**
†These authors contributed equally to this work.

Corrected 22 December 2021. See full text.

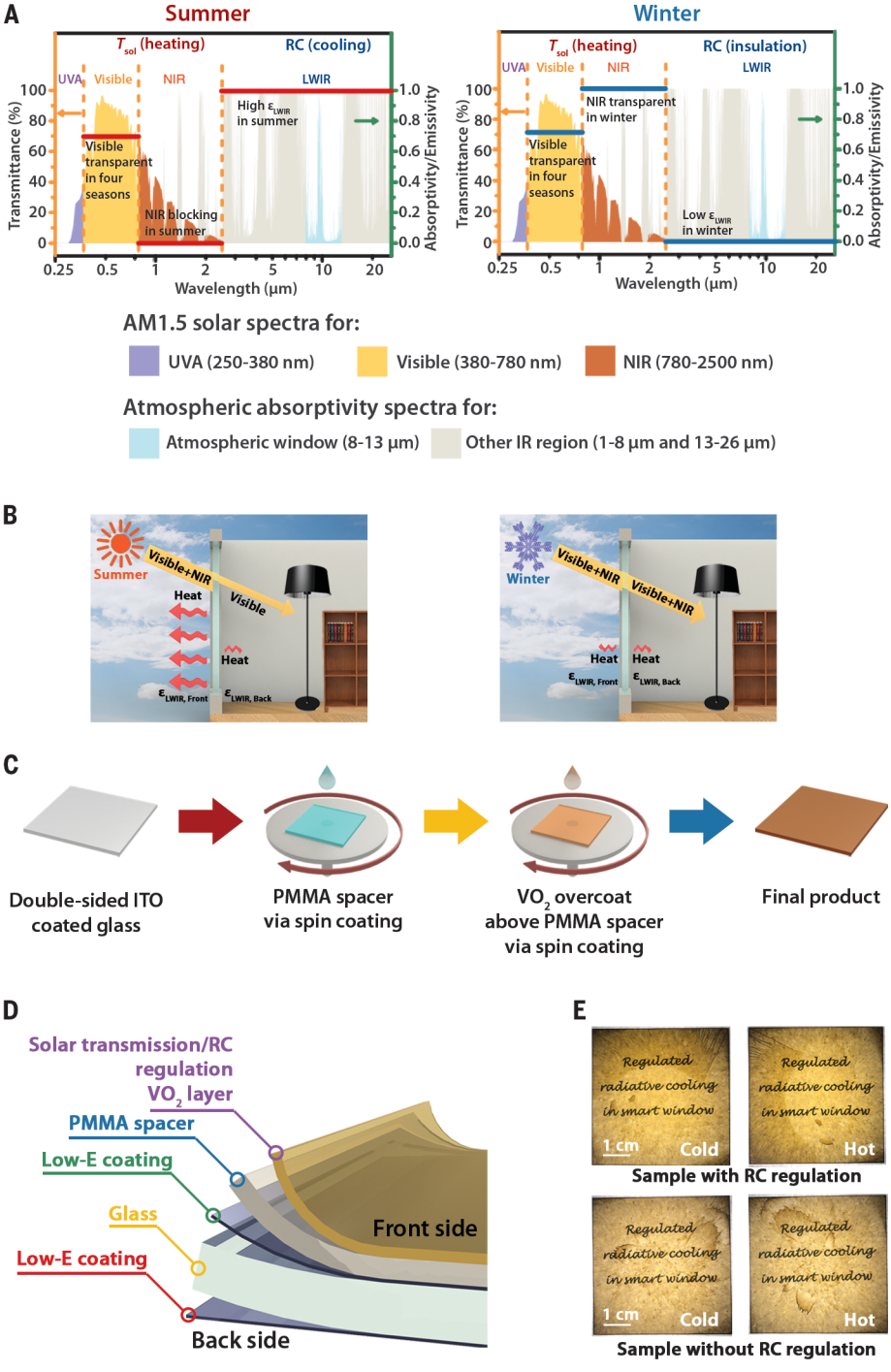

Fig. 1. Structure and concept of an RCRT window. (**A**) Concept of the ideal energy-saving smart window. The red and blue lines represent the spectra for an ideal energy-saving smart window in summer and winter. T_{sol} and thermal radiation in LWIR contribute to heating and cooling, respectively. Visible transparency remains constant. Windows should be NIR blocking and have high $\varepsilon_{LWIR\text{-}H}$ to promote radiative cooling in summer, and the response must be switched to the opposite in the winter. (**B**) Working principle of RCRT window in summer (left) and winter (right). The yellow arrows indicate the T_{sol} and the red arrows represent heat radiation. In summer, the NIR is blocked and visible light transmits through the window with thermal radiation enhanced. In winter, both NIR and visible light enter the room. Heat radiation is suppressed to minimize heat loss. (**C**) Schematics of the fabrication process for the RCRT window. (**D**) Schematic structure of the RCRT window. (**E**) Photos of the RCRT window with RC regulation (top) and the VO_2 window without RC regulation (bottom) at low and high temperature. The size of samples is 5 × 5 cm.

We systematically studied the tunability of the ε_{LWIR} of RCRT window by adjusting the thickness of the PMMA spacer and the VO_2 nanoparticle weight ratio in the overcoat. We established a relationship among PMMA thickness, VO_2 weight ratio, and ε_{LWIR} (fig. S9). By fixing a VO_2 weight ratio of 20:1, $\Delta\varepsilon_{LWIR}$ gradually increased from 0.28 to the maximum of 0.4 and dropped to 0.08 with increasing spacer thickness. We observed a similar trend of $\Delta\varepsilon_{LWIR}$ relating to spacer thickness in our optical simulation using the finite difference time domain method with the VO_2 layer, PMMA spacer, and double-sided ITO glass (fig. S10). Three representative samples are presented, along with their spectra, using different ε_{LWIR} modulation abilities, max $\Delta\varepsilon$ ($\varepsilon_{LWIR\text{-}L}$=0.21 and $\varepsilon_{LWIR\text{-}H}$ = 0.61), max ε ($\varepsilon_{LWIR\text{-}L}$ = 0.47 and $\varepsilon_{LWIR\text{-}H}$ = 0.67), and min ε ($\varepsilon_{LWIR\text{-}L}$ = 0.13 and $\varepsilon_{LWIR\text{-}H}$ = 0.36) (Fig. 3A).

To evaluate the impact of T_{sol} and ε_{LWIR} in different climate zones (*32*), we mapped the heating and cooling energy consumption per window area versus T_{sol} (10 to 90%) and ε_{LWIR} (0.1 to 0.9) across seven climate zones (Fig. 3B for zone 4 and figs. S12 to S17 for the rest of the zones). In our simulation, we used a single-story small office building as a prototype (fig. S11 and table S2A). We observed that in all seven zones, the minimum energy consumption (E_{min}) for cooling happened at T_{sol} = 10% and ε_{LWIR} = 0.9, and the E_{min} for heating occurred at ε_{LWIR} = 0.1 and T_{sol} = 90%. This agrees well with our proposed ideal window (Fig. 1A).

To further investigate the importance of RC regulation, we fixed T_{sol} to 30% for building energy simulation, considering that the building energy standard of American Society of Heating, Refrigerating, and Air-Conditioning Engineers (ASHRAE) recommends the assembly maximum solar heat gain coefficient of 0.21 to 0.40 for climate zones 1 to 7. (*32*) We summarized the total E_{min} by adding heating and cooling from mappings (table S4), and the best-performing static ε_{LWIR} was 0.9 for zones 1 to 4 and 0.1 for the colder zones 6 to 7 (Fig. 3C and fig. S18). Comparatively, the dynamic ε_{LWIR} sample (ε_{LWIR} of 0.9 for cooling and ε_{LWIR} of 0.1 for heating) was able to save up to 115.9 MJ m^{-2} energy annually compared with the best-performing static ε_{LWIR} samples. This comparison demonstrates the capability of a dynamic ε_{LWIR} modulation window to cater the energy-saving demand in different climates.

We conducted energy consumption simulation of a full-scale building with the model of a typical 12-story large office building with a floor dimension of 73 m (240 ft) length × 49 m (160 ft) width × 4 m (13 ft) height and a total window glass area of 4636 m^2 (fig. S19 and table S2B). Whereas the RCRT window with pure VO_2 had a high τ_c of ~60°C, a tungsten-doped VO_2 (W-doped VO_2) max $\Delta\varepsilon$ window, with its low τ_c of ~27.5°C (fig. S20 and table

Corrected 22 December 2021. See full text.

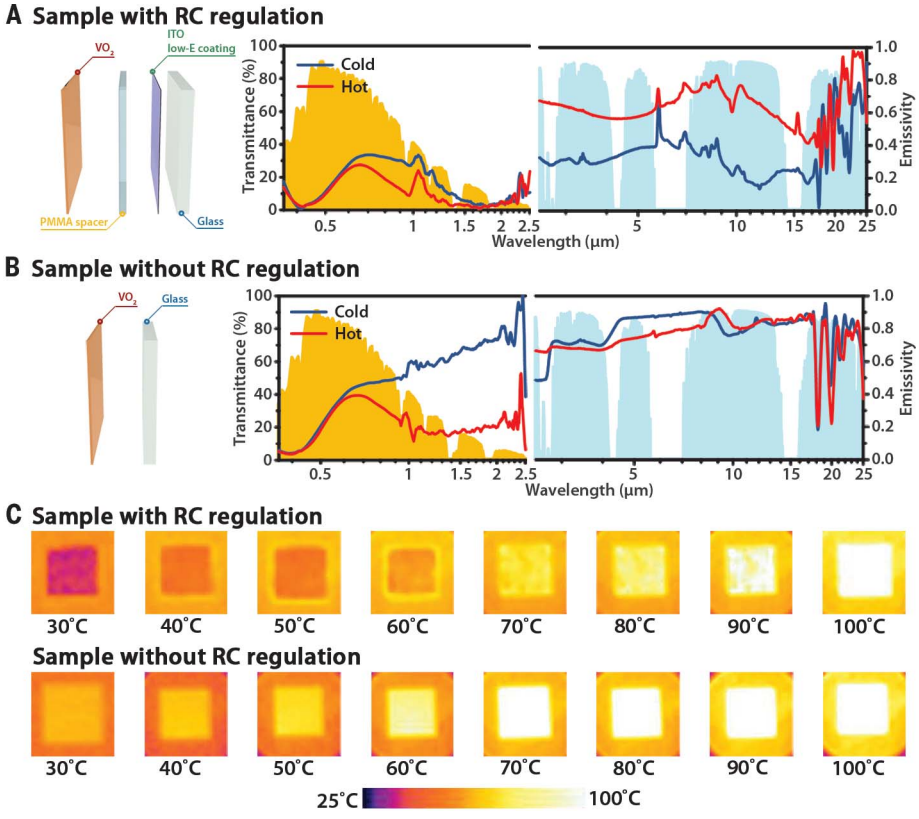

Fig. 2. Optical and thermal performance of the RCRT window. (**A** and **B**) Spectra of the sample with (A) and without (B) RC regulation in the visible-NIR and LWIR range at 20°C (blue line) and 90°C (red line) against a normalized AM1.5 global solar spectrum (yellow shadow) and LWIR atmospheric transmittance window (blue shadow), respectively. The schematics on the left illustrate the structure of the samples with and without RC regulation, respectively. Both samples give solar modulation, but the RCRT window shows a low ε_{LWIR} at 20°C and a high ε_{LWIR} at 90°C, whereas the ε_{LWIR} change for the sample without RC regulation is small. (**C**) IR camera image of the RCRT window (top) and the VO_2 sample without RC regulation (bottom) with temperature increasing from 30° to 100°C. The ε_{LWIR} for background is 0.5. The darker color of the sample with RC regulation compared with background from 30 to 60°C indicates that its ε_{LWIR} is <0.5, whereas a brighter color from 70° to 100°C indicates that ε_{LWIR} switches >0.5. By contrast, from 30° to 100°C, the sample without RC regulation is brighter than the background.

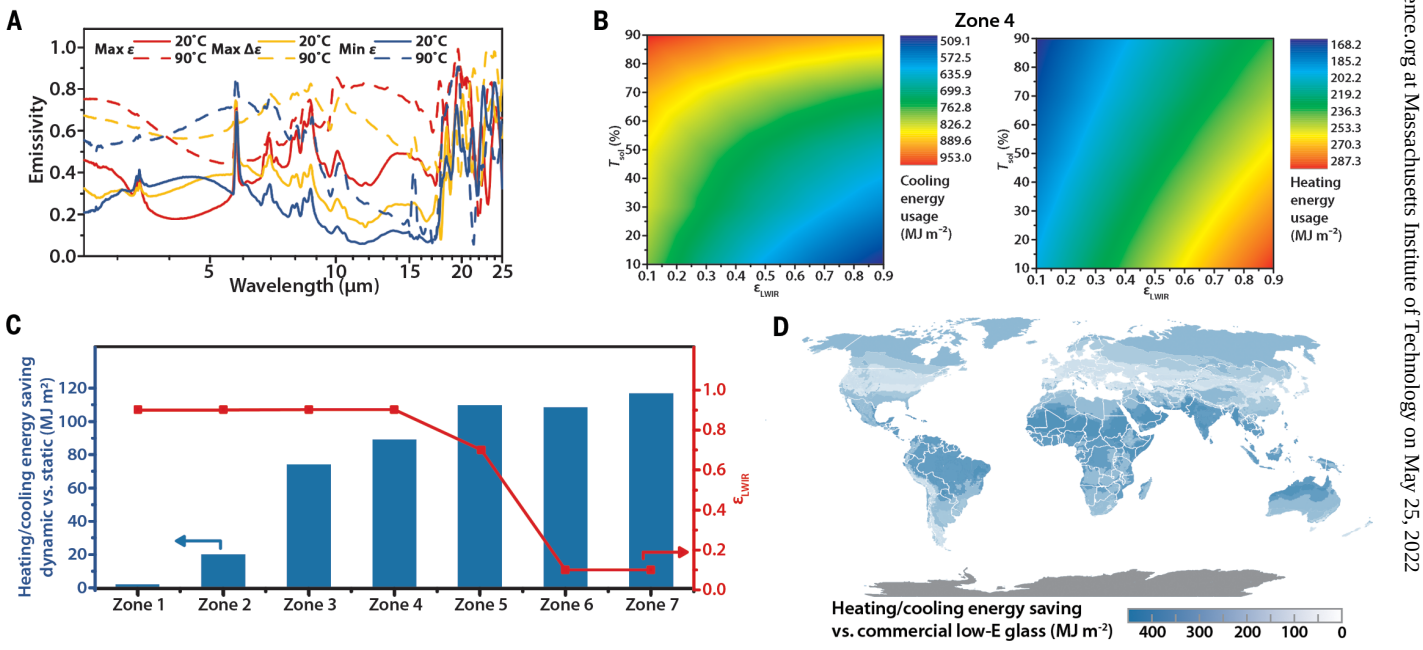

Fig. 3. ε_{LWIR} emissivity regulation and energy consumption simulation for the RCRT window. (**A**) $\varepsilon_{LWIR\text{-}L}$ (solid line) and $\varepsilon_{LWIR\text{-}H}$ (dotted line) spectra for max ε (red line), max Δε (yellow line), and min ε (blue line) VO_2 RCRT samples, respectively. The samples with different ε_{LWIR} regulation abilities were fabricated by varying the thickness of PMMA spacer while fixing the thickness of VO_2-PMMA layer and the VO_2 weight ratio. (**B**) Mapping result on the effects of T_{sol} and ε_{LWIR} to the cooling (left) and heating (right) energy usage in climate zone 4. The minimum energy consumption for cooling happens at ε_{LWIR} = 0.9 and T_{sol} = 10%, and the minimum energy consumption for heating happens at the point with ε_{LWIR} = 0.1 and T_{sol} = 90%. This observation agrees well with the proposed ideal window in Fig. 1A. (**C**) Heating and cooling energy saving (blue columns) of simulated optimized dynamic samples against optimized static samples (red square) from zones 1 to 7. In this simulation, T_{sol} was fixed to 30%. The optimized static ε sample is derived from the point of minimum total energy consumption by adding heating and cooling in seven climate zones by fixing ε. The optimized dynamic ε window has a ε_{LWIR} of 0.9 for cooling and 0.1 for heating. The optimized dynamic ε window has lower energy consumption than optimized static ε window from zones 2 to 7. (**D**) Estimated world heating and cooling energy-saving of a W-doped max Δε sample against a commercial low-E glass as the baseline. RCRT windows outperform the commercial low-E across different climate zones. Unit for the energy-saving is MJ m^{-2}.

S3), has been instead applied in the full-scale building energy simulation. The optical response from 20° to 60°C with the interval of 10°C was used in the simulations (fig. S21). It should be noted that broadband cooler with high emssivity over the infrared spectra at 3-30 μm had a larger net cooling power than the 8- to 13-μm selective cooler when the surface temperature was above or close to the surrounding ambient temperature. (*33*) In the daytime, the exterior surface temperature of window glass is generally higher than the ambient temperature (fig. S22); therefore, we used the broadband emission in our calculations. We compared the energy-saving performance of the W-doped max $\Delta\varepsilon$ RCRT sample in different climate zones with a commercial low-E window and a conventional thermochromic window without RC regulation (fig. S23 and table S5). Our RCRT sample yielded a higher energy-saving performance benchmarked by a commercial low-E glass across all different climate zones (Fig. 3D), with energy saving up to 324.6 MJ m^{-2}, which further shows the potential importance of RC regulation and solar modulation in windows.

In summary, we fabricated a thermochromic smart window with tunable ε_{LWIR} based on a W-doped VO_2-PMMA/spacer/low-E stack using a solution process to cater to the dynamic energy demand in different climate zones. The ε_{LWIR} modulation ability of the windows can be tuned by simply adjusting the spacer thickness and VO_2 weight ratio and doping. In the whole-building energy simulations, the RCRT window showed a higher heating and cooling energy savings than a commercial low-E glass across the different climate zones. This type of technology has the potential to cut down the carbon emissions related to heating and cooling, improving the sustainability of buildings. Passive ε_{LWIR} and solar modulation has the potential to be useful for a wide range of heat-regulating applications including windows, walls, roofs, fabrics, and paintings.

REFERENCES AND NOTES

1. L. Zhao, X. Lee, R. B. Smith, K. Oleson, *Nature* **511**, 216–219 (2014).
2. E. Cuce, S. B. Riffat, *Renew. Sustain. Energy Rev.* **41**, 695–714 (2015).
3. Y. Gao *et al*., *Energy Environ. Sci.* **5**, 8234–8237 (2012).
4. E. S. Lee, X. Pang, S. Hoffmann, H. Goudey, A. Thanachareonkit, *Sol. Energy Mater. Sol. Cells* **116**, 14–26 (2013).
5. Y. Y. Cui *et al*., *Joule* **2**, 1707–1746 (2018).
6. Y. Ke *et al*., *Adv. Energy Mater.* **9**, 1902066 (2019).
7. S. Wang *et al*., *Appl. Energy* **211**, 200–217 (2018).
8. C. G. Granqvist, *Phys. Scr.* **32**, 401–407 (1985).
9. A. P. Raman, M. A. Anoma, L. Zhu, E. Rephaeli, S. Fan, *Nature* **515**, 540–544 (2014).
10. L. Zhu, A. P. Raman, S. Fan, *Proc. Natl. Acad. Sci. U.S.A.* **112**, 12282–12287 (2015).
11. Z. Chen, L. Zhu, A. Raman, S. Fan, *Nat. Commun.* **7**, 13729 (2016).
12. B. Bhatia *et al*., *Nat. Commun.* **9**, 5001 (2018).
13. J. Mandal *et al*., *Joule* **3**, 3088–3099 (2019).
14. L. Zhou *et al*., *Nat. Sustain.* **2**, 718–724 (2019).
15. Y. Zhai *et al*., *Science* **355**, 1062–1066 (2017).
16. D. Zhao *et al*., *Joule* **3**, 111–123 (2019).
17. E. A. Goldstein, A. P. Raman, S. Fan, *Nat. Energy* **2**, 17143 (2017).
18. Z. Chen, L. Zhu, W. Li, S. Fan, *Joule* **3**, 101–110 (2019).
19. Y. Peng *et al*., *Nat. Sustain.* **1**, 105–112 (2018).
20. T. Li *et al*., *Science* **364**, 760–763 (2019).
21. J. Mandal *et al*., *Science* **362**, 315–319 (2018).
22. H. Ye, X. Meng, B. Xu, *Energy Build.* **49**, 164–172 (2012).
23. H. Ye, X. Meng, L. Long, B. Xu, *Renew. Energy* **55**, 448–455 (2013).
24. M. Ono, K. Chen, W. Li, S. Fan, *Opt. Express* **26**, A777–A787 (2018).
25. C. Xu, M. Colorado Escobar, A. A. Gorodetsky, *Adv. Mater.* **32**, e1905717 (2020).
26. L. Xiao *et al*., *Nano Lett.* **15**, 8365–8370 (2015).
27. M. Li, D. Liu, H. Cheng, L. Peng, M. Zu, *Sci. Adv.* **6**, eaba3494 (2020).
28. Y. Ke *et al*., *Adv. Funct. Mater.* **28**, 1800113 (2018).
29. Y. Zhou *et al*., *Joule* **4**, 2458–2474 (2020).
30. M. A. Kats *et al*., *Appl. Phys. Lett.* **101**, 221101 (2012).
31. S. Taylor, Y. Yang, L. Wang, *J. Quant. Spectrosc. Radiat. Transf.* **197**, 76–83 (2017).
32. ANSI/ASHRAE/IES, "Energy standard for buildings except low-rise residential buildings" (ANSI/ASHRAE/IES, 2019); https://www.ashrae.org/technical-resources/bookstore/standard-90-1.
33. X. Yin, R. Yang, G. Tan, S. Fan, *Science* **370**, 786–791 (2020).

ACKNOWLEDGMENTS

Funding: The research was supported by the National Research Foundation, Prime Minister's Office, Singapore, under its Campus for Research Excellence and Technological Enterprise (CREATE) program and by the Singapore-HUJ Alliance for Research and Enterprise (SHARE), the Sino-Singapore International Joint Research Institute (SSIJRI), and Singapore Ministry of Education (MOE) Academic Research Fund Tier One RG103/19. **Author contributions:** Y.L. proposed, designed, and guided the project as principal investigator. S.W. fabricated the samples, performed the optical and thermal analyses, and drafted the manuscript with others. T.J. performed energy-saving performance simulation under the guidance of G.T. Y.M. performed theoretical simulation for the optical properties. Y.L., R.Y., and G.T. discussed and revised the manuscript. All authors checked the manuscript. **Competing interests:** A Singapore provisional patent (10202112639V) related to this work has been filed by Y.L. and S.W. **Data and materials availability:** All data are available in the main text or the supplementary materials.

SUPPLEMENTARY MATERIALS

science.org/doi/10.1126/science.abg0291
Materials and Methods
Figs. S1 to S27
Tables S1 to S6
References (*34*–*67*)

6 December 2020; accepted 26 October 2021
10.1126/science.abg0291

Science

Scalable thermochromic smart windows with passive radiative cooling regulation

Shancheng WangTengyao JiangYun MengRonggui YangGang TanYi Long

Science, 374 (6574), • DOI: 10.1126/science.abg0291

A passive turnoff

Passive radiative cooling technology uses the infrared atmospheric window to allow outer space to be a cold sink for heat. However, this effect is one that is only helpful for energy savings in the warmer months. Wang *et al*. and Tang *et al*. used the metal-insulator transition in tungsten-doped vanadium dioxide to create window glass and a rooftop coating that circumvents this problem by turning off the radiative cooling at lower temperatures. Because the transition is simply temperature dependent, this effect also happens passively. Model simulations suggest that these materials would lead to energy savings year-round across most of the climate zones in the United States. —BG

Science (ISSN) is published by the American Association for the Advancement of Science. 1200 New York Avenue NW, Washington, DC 20005. The title *Science* is a registered trademark of AAAS.